Generalized Mass-Transfer Correction Factor for Nanofiltration and Reverse Osmosis

Vítor Geraldes and Maria Diná Afonso
Dept. of Chemical and Biological Engineering, Instituto Superior Técnico, 1049-001 Lisbon, Portugal

DOI 10.1002/aic.10968
Published online August 23, 2006 in Wiley InterScience (www.interscience.wiley.com).

The assessment of the concentration polarization in pressure-driven membrane modules is fundamental for their design and optimization. To account for the suction effect in nanofiltration (NF)/reverse osmosis (RO) membrane modules, a correction factor for conventional mass-transfer coefficients at vanishing mass-transfer rates was obtained through computational fluid dynamics (CFD) simulations of a symmetrical NF/RO rectangular channel with fully developed laminar flow, for a wide range of operating conditions. The correction factor is defined as $\Xi = Sh/Sh^0$*, where Sh is the Sherwood number with suction and* Sh^0 *is the Sherwood number for impermeable walls and low mass-transfer rates. For the range of dimensionless numbers assigned in the simulations, it was found by fitting of CFD data that* Ξ *depends only on* $\phi = Pe/Sh^0$*, through the correlation* $\Xi = \phi + (1 + 0.26\phi^{1.4})^{-1.7}$*, where Pe is the permeation Peclet number. This correlation can be used to predict the average concentration polarization index,* $\bar{\Gamma} = R/(\Xi/\phi - R)$*, where R is the intrinsic rejection, with an average relative error of 3.2%. The correlation obtained appears to be suitable to determine mass-transfer coefficients at high mass-transfer rates, independently of the membrane module geometry and the flow regime. Moreover, unlike the correction factor correlations available in the literature, the generalized correlation accurately predicts the concentration polarization index for* $\phi < 20$*.* © 2006 American Institute of Chemical Engineers *AIChE J,* 52: 3353–3362, 2006
Keywords: computational fluid dynamics (CFD), concentration polarization index, mass-transfer correction factor, NF/RO membrane modules, suction

Introduction

It is well known that the prediction of the solute concentration at the membrane surface is a fundamental step in the design, control, and optimization of pressure-driven membrane modules. The simplest and yet most useful methodology for such a purpose is based on film theory.[1-3] Film theory is appealing from the designer's perspective because it is simple and makes use of well-known mass-transfer correlations. However, the latter were determined for systems with identical geometries but impermeable walls and low mass-transfer rates, and it has been argued that for pressure-driven membrane modules, the hydraulic permeabilities are too high to rely on mass-transfer coefficients at low mass-transfer rates.[4-6] Meanwhile, it has been shown[7-9] that film theory is suitable for predicting the concentration polarization index for small indexes and a tight range of nanofiltration (NF)/reverse osmosis (RO) operating conditions. However, the validity range of film theory has not been clearly defined and no extended simple correlation has been proposed so far.

The prediction of the concentration polarization index for typical operating conditions in NF/RO membrane modules has been accomplished by computational fluid dynamics.[10-12] Nevertheless, the complexity, time consumption, and large amount of generated data associated with computational fluid dynamics (CFD) makes difficult its direct use for predicting the concentration polarization index in expedited module design, control, and optimization. An alternative and more efficient use of CFD

Correspondence concerning this article should be addressed to V. Geraldes at vitor.geraldes@ist.utl.pt.

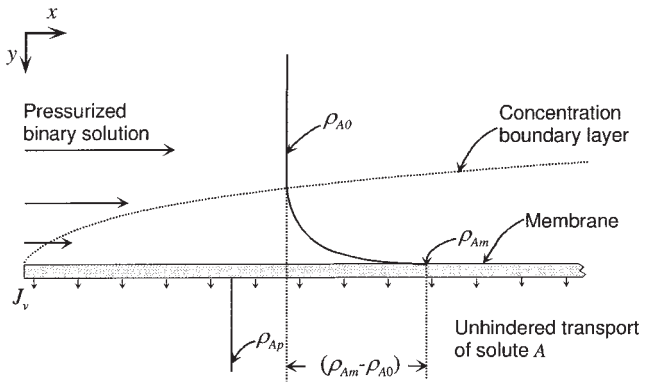

Figure 1. Mass transport of solute *A* and solvent *B* at the vicinity of a semipermeable membrane.

is to predict the concentration polarization index and mass-transfer coefficients for a broad range of typical operating conditions and subsequently to determine dimensionless mass-transfer correlations.

In the present work, CFD was used to predict the velocity and concentration profiles in a rectangular slit with fully developed laminar flow of binary solutions along two parallel semipermeable membranes, for a broad range of typical NF/RO operating conditions. A correction factor to account for the suction effect on conventional mass-transfer coefficients was determined from each simulation and a generalized semiempirical correlation was fitted to CFD data.

This work shows that the concentration polarization index can be simply predicted by correcting the mass-transfer coefficients at low mass-transfer rates, through a generalized correction factor that depends only on the ratio Pe/Sh^0, where Pe is the permeation Peclet number and Sh^0 is the Sherwood number at impermeable walls and low mass-transfer rates. This mass-transfer correction factor predicts the concentration polarization data available in the literature for similar conditions and it also appears suitable for tubular and radial geometries and turbulent flow, as well.

Theory

Let us assume that a pressurized binary solution bearing a given mass concentration of solute A, ρ_{A0}, flows along a membrane module channel with arbitrary geometry (Figure 1). Assuming that the water recovery rate is low, the thickness of the concentration boundary layer is much smaller than the channel height, and thus the bulk concentration of solute A along the channel remains nearly constant ($\approx\rho_{A0}$). The solvent B permeates preferentially through the membrane, whereas the solute A is partially or completely retained. Thereupon, the buildup of a concentration distribution of solute A occurs at the membrane vicinity, the mass concentration of A at the membrane surface, ρ_{Am}, being higher than ρ_{A0}. Neglecting end effects, the concentration profile developed at the membrane vicinity depends only on the distance to the channel inlet and the distance to the membrane surface. Figure 1 depicts the mass transfer and the concentration profile of solute A in the feed channel of a membrane module, at an arbitrary distance from the inlet. On the other hand, there is no resistance to the transport of solute A across the membrane, that is, unhindered transport is assumed.

The membrane selectivity may be assessed by the intrinsic rejection R, which is assumed to be independent of x, and/or the average observed rejection R_{obs},* the definitions of which are

$$R = (\rho_{Am} - \rho_{Ap})/\rho_{Am} = (\bar{\rho}_{Am} - \bar{\rho}_{Ap})/\bar{\rho}_{Am} \tag{1}$$

$$R_{obs} = (\rho_{A0} - \bar{\rho}_{Ap})/\rho_{A0} \tag{2}$$

where $\bar{\rho}_{Am}$ and $\bar{\rho}_{Ap}$ are the permeate flux averages of the mass concentration of A at the membrane surface and in the permeate stream, respectively (see Appendix A, Eqs. A3 and A4). Obviously, the average observed rejection is lower than the intrinsic rejection.

On the other hand, the concentration polarization may be assessed by the average concentration polarization index:

$$\bar{\Gamma} = (\bar{\rho}_{Am} - \rho_{A0})/\rho_{A0} \tag{3}$$

Combining Eqs. 1–3 yields a relation between R, R_{obs}, and $\bar{\Gamma}$:

$$\bar{\Gamma} = \frac{R - R_{obs}}{1 - R} \tag{4}$$

Bearing in mind that the mass concentration of solute A at the membrane surface varies in the x-direction, it is convenient to define an average mass-transfer coefficient k_ρ:

$$\bar{j}_{Am} = -k_\rho(\bar{\rho}_{Am} - \rho_{A0}) \tag{5}$$

where $\bar{j}_{Am}$ is the permeate flux-average back-diffusion flux of solute A normal to the membrane surface between $x = 0$ and $x = L$, given by (see Appendix A, Eq. A5)

$$\bar{j}_{Am} = -\bar{J}_v(\bar{\rho}_{Am} - \bar{\rho}_{Ap}) \tag{6}$$

where $\bar{J}_v$ is the average permeate flux. Equating Eqs. 5 and 6 leads to the expression of the average mass-transfer coefficient:

$$k_\rho = \bar{J}_v \frac{(\bar{\rho}_{Am} - \bar{\rho}_{Ap})}{(\bar{\rho}_{Am} - \rho_{A0})} \tag{7}$$

and by multiplying both terms of Eq. 7 by h/D_{AB}, where h is a characteristic length and D_{AB} is the mass diffusivity, the following equation is obtained:

$$Sh = Pe \frac{(\bar{\rho}_{Am} - \bar{\rho}_{Ap})}{(\bar{\rho}_{Am} - \rho_{A0})} \tag{8}$$

where $Sh = k_\rho h/D_{AB}$ is the average Sherwood number and $Pe = \bar{J}_v h/D_{AB}$ is the average permeation Peclet number. Combining Eqs. 2, 3, and 8, leads to

* The local observed rejection varies in the x-direction as a result of the variation of ρ_{Ap}.

$$\bar{\Gamma} = \frac{R_{obs}}{\text{Sh/Pe} - 1} \tag{9}$$

Because the intrinsic rejection is assumed to be independent of x, the permeate flux-average mass concentration of A in the permeate stream, $\bar{\rho}_{Ap}$, is given by Eq. 1:

$$\bar{\rho}_{Ap} = (1 - R)\bar{\rho}_{Am} \tag{10}$$

By combining Eqs. 3, 8, and 10 and rearranging, the following equation is obtained:

$$\bar{\Gamma} = \frac{R}{\text{Sh/Pe} - R} \tag{11}$$

To develop physically consistent Sh correlations, it is essential to analyze the structure of Eqs. 9 and 11. According to Eq. 9, the ratio Sh/Pe must be >1 such that the concentration polarization indexes are not negative. On the other hand, as the permeation Peclet number increases, $\bar{\rho}_{Am}$ increases, and given that R is assumed to be constant, $\bar{\rho}_{Ap}$ increases, and thus R_{obs} decreases. When Pe becomes very large, R_{obs} vanishes and the concentration polarization index $\bar{\Gamma}$ reaches a maximum: $\bar{\Gamma}_{\max} = R/(1 - R)$ (see Eq. 4). Therefore, Eq. 11 requires that Sh/Pe $\rightarrow 1$ as Pe $\rightarrow \infty$. Besides these two restrictions of Sh/Pe, another one results from the fact that the Sherwood number becomes independent of the permeation velocity (and therefore of Pe), for low mass-transfer rates (low Pe) at the membrane surface.[13] Defining Sh^0 as the Sherwood number for vanishing mass-transfer rates at the membrane surface, Sh $\rightarrow \text{Sh}^0$ as Pe $\rightarrow 0$. A postulated correlation that satisfies the aforementioned restrictions is

$$\text{Sh} = \text{Pe} + \frac{\text{Sh}^0}{[1 + \xi(\text{Pe/Sh}^0)]^{c_1}} \tag{12}$$

where c_1 is a positive fitting parameter and ξ is a function that satisfies the asymptotic conditions $\xi \rightarrow 0$ as Pe $\rightarrow 0$ and $\xi \rightarrow \infty$ as Pe $\rightarrow \infty$. An appropriate function, $\xi = c_2(\text{Pe/Sh}^0)^{c_3}$, with positive fitting parameters c_2 and c_3, was selected by trial and error. By defining $\phi = \text{Pe/Sh}^0$ and $\Xi = \text{Sh/Sh}^0$ as the correction factor for Sh^0 to obtain Sh at high mass-transfer rates (that is, to take into account the effect of suction in NF/RO systems), the following equation is obtained after dividing Eq. 12 by Sh^0:

$$\Xi = \phi + \frac{1}{[1 + \xi(\phi)]^{c_1}} = \phi + \frac{1}{(1 + c_2\phi^{c_3})^{c_1}} \tag{13}$$

Thereby, the average Sherwood number for a given membrane module consists of the product of Sh^0 by the correction factor $\Xi(\phi)$. Once Sh^0 and $\Xi(\phi)$ are known, the concentration polarization index can easily be determined by

$$\bar{\Gamma} = \frac{R}{\Xi/\phi - R} \tag{14}$$

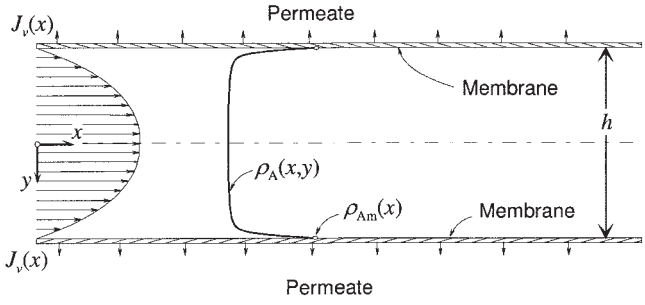

Figure 2. Thin rectangular channel formed by two flat parallel identical NF/RO membranes.

Case Study

The reverse osmosis/nanofiltration system studied is schematically shown in Figure 2. A binary solution under pressure P_0, bearing a given mass concentration ρ_{A0}, and osmotic pressure π_0, flows in steady fully developed laminar regime inside a channel of height h and length L, formed by two flat parallel identical membranes, the intrinsic rejection of which is assumed to be independent of x. The physical properties of the binary solution are assumed to be constant and the osmotic pressure π is assumed to be proportional to the solute mass concentration, that is, $\pi = b\rho_A$. The pure water hydraulic permeability is L_p. The transmembrane pressure ΔP is assumed to be constant along the channel, given that the pressure drop for laminar flow along short channels is negligible. Because the channel height is much smaller than its width, the velocity distribution inside the channel is two-dimensional. At the channel inlet, the velocity profile $u(y)$ is assumed to be parabolic, the average velocity being u_0.

For this system, the continuity, Navier–Stokes, and solute continuity equations are

$$\frac{\partial u}{\partial x} + \frac{\partial v}{\partial y} = 0 \tag{15}$$

$$\rho\left(u\frac{\partial u}{\partial x} + v\frac{\partial u}{\partial y}\right) = -\frac{\partial P}{\partial x} + \mu\left(\frac{\partial^2 u}{\partial x^2} + \frac{\partial^2 u}{\partial y^2}\right) \tag{16}$$

$$\rho\left(u\frac{\partial v}{\partial x} + v\frac{\partial v}{\partial y}\right) = -\frac{\partial P}{\partial y} + \mu\left(\frac{\partial^2 v}{\partial x^2} + \frac{\partial^2 v}{\partial y^2}\right) \tag{17}$$

$$u\frac{\partial \rho_A}{\partial x} + v\frac{\partial \rho_A}{\partial y} = D_{AB}\left(\frac{\partial^2 \rho_A}{\partial x^2} + \frac{\partial^2 \rho_A}{\partial y^2}\right) \tag{18}$$

and the boundary conditions are

- at $y = h/2$ and $x > 0$

$$u = 0 \qquad v \equiv J_v = L_p(\Delta P - b\rho_{Am}R) \qquad D_{AB}\partial\rho_A/\partial y = J_v\rho_{Am}R \tag{19a,b,c}$$

- at $y = 0$ and $x > 0$

$$\partial u/\partial y = 0 \qquad v = 0 \qquad \partial\rho_A/\partial y = 0 \tag{20a,b,c}$$

- at $x = 0$ and $0 < y < h/2$

$$u = \frac{3}{2} u_0[1 - (2y/h)^2] \qquad v = 0 \qquad \rho_A = \rho_{A0} \qquad P = P_0 \tag{21a,b,c,d}$$

- at $x = L$ and $0 < y < h/2$

$$\partial u/\partial x \approx 0 \qquad \partial v/\partial x = 0 \qquad \partial \rho_A/\partial x \approx 0 \tag{22a,b,c}$$

Equations 22a–22c are typical outflow boundary conditions for parabolic flows that are widely used in the literature.[14] The flow is parabolic at the outlet because the flow is already fully developed at the channel entrance and the permeation velocity is several orders of magnitude lower than the longitudinal velocity. Equations 22a and 22c are further discussed in the next section.

The dimensionless analysis presented in Appendix B shows that the dimensionless mass concentration of solute A at the membrane surface ($y^* = \pm 1/2$) depends on R, x^* (dimensionless distance to the channel inlet), $\mathrm{Re} = \rho u_0 h/\mu$ (Reynolds number at the channel inlet), $\mathrm{Sc} = \mu/(\rho D_{AB})$ (Schmidt number), $\Pi_J = L_p \Delta P/u_0$ (dimensionless pure water flux), and $\Pi_P = \pi_0/\Delta P$ (dimensionless osmotic pressure). Thus, the average concentration polarization index and the average Sherwood number (Eqs. 3 and 8) between $x^* = 0$ and $x^* = L/h$ are also correlated with these dimensionless numbers, that is, both $\bar{\Gamma}$ and Sh are functions of R, L/h, Re, Sc, Π_J, and Π_P.

CFD numerical method

The transport equations (Eqs. 15–18), together with suitable boundary conditions (Eqs. 19–22), were solved by the control volume approach, using the SIMPLE algorithm to deal with the pressure–velocity coupling.[14] The bulk flow terms in the transport equations were discretized using the hybrid scheme, which switches between the upwind and the central differences schemes depending on the local grid Peclet number. The algebraic equations generated by the control volume integration were solved by the tridiagonal matrix algorithm.[14] A structured grid containing 75 nodes in the x-direction and 75 nodes in the y-direction were found to be fine enough to yield grid independent results. The grid density was higher near the membrane surface where steeper concentration gradients occur.

Given that the flow is parabolic at the outlet, the variables at this boundary do not affect the upstream variables. In the numerical method, the velocities and the concentration at the outlet are equal to the corresponding values in the last column of nodes, and a small correction is made on u and ρ_A to take into account the permeation through the membrane and close the overall mass balances. Thus, the derivatives $\partial u/\partial x$ and $\partial \rho_A/\partial x$ in Eqs. 22a and 22c are only approximately null.

Table 1. Dimensionless Numbers Assigned in the CFD Simulations

Sc	Re	L/h	R	Π_P	$\Pi_J/\Pi_{J,\max}$
300	30	3	0.10	0.0	0.003
1000	100	10	0.50	0.01	0.01
3000	300	30	0.90	0.03	0.03
	1000	100	0.97	0.1	0.1
		300	0.99	0.5	0.3
			0.999	0.9	1.0
			1.0		

Note: $\Pi_{J,\max}$ is the maximum of $0.2/[\mathrm{Re}(1 - \Pi_P R)]$ and $0.3/[2(L/h)(1 - \Pi_P R)]$.

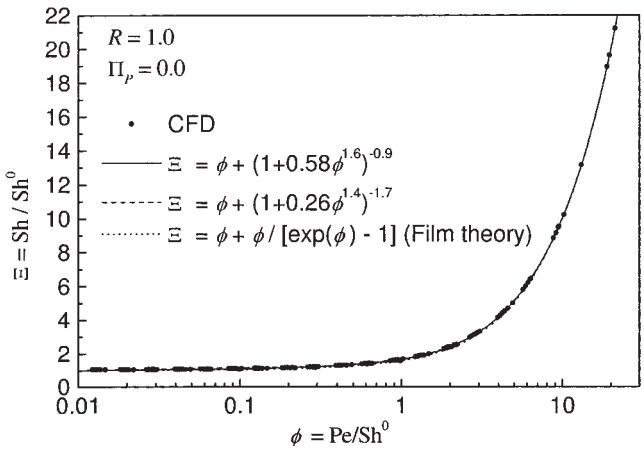

Figure 3. CFD predictions (points) of Ξ vs. ϕ for $R = 1.0$, $\Pi_P = 0.0$, and the dimensionless numbers (Re, Sc, L/h, Π_J) listed in Table 1, together with empirical correlations.

The CFD numerical method was described in detail elsewhere.[15] That work showed that the CFD predictions of the velocities distributions and the average concentration polarization index in an NF rectangular slit with fully developed laminar flow and constant permeation flux agreed with benchmark theoretical solutions of Benman[16]and Sherwood et al.,[1] respectively. Furthermore, the predicted rejections matched the experimental (observed) rejections of sodium chloride solutions.[15]

CFD simulations design

The CFD simulations were carried out for all combinations of the dimensionless numbers listed in Table 1, in a total number of 15,120. The Schmidt numbers assigned in the CFD simulations (300–3000) are typical of aqueous solutions of inorganic salts and organic compounds of molecular weights in the range 300–1000 Dalton. The highest Reynolds number assigned (1000) is lower than the critical Reynolds number for steady laminar flow of Newtonian fluids in thin rectangular channels (1400).[17] The dimensionless distance to the channel inlet, L/h, ranged from 3 to 300, values typical of distinct types of feed channels. The dimensionless numbers R and Π_P ranged from 0.1 to 1.0 and 0.0 to 0.9, respectively. The dimensionless number Π_J was limited by the maximum inlet permeation Reynolds number, $\mathrm{Re}_{p0} = \rho h J_{v0}/\mu$, and the maximum water recovery rate (based on the inlet permeation flux), $\Delta_0 = 2J_{v0}L/(u_0 h)$. The maximum inlet permeation Reynolds number is determined by the membrane structure, whereas the maximum water recovery rate is determined by the membrane structure, as well as the crossflow velocity inside the channel and the

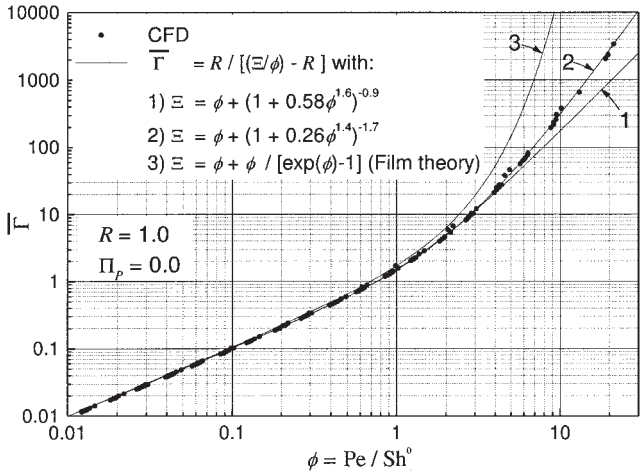

Figure 4. CFD predictions (points) of $\bar{\Gamma}$ vs. ϕ for $R = 1.0$, $\Pi_P = 0.0$, and the dimensionless numbers (Re, Sc, L/h, Π_J) listed in Table 1, together with empirical correlations.

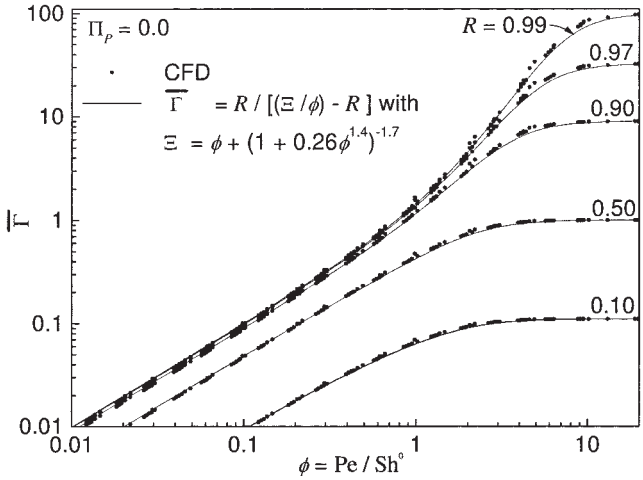

Figure 5. Comparison of $\bar{\Gamma}$ predicted by Eq. 23 with the CFD predictions (points) for $\Pi_P = 0.0$, $0.10 \leq R \leq 0.99$, and the dimensionless numbers (Re, Sc, L/h, Π_J) listed in Table 1.

channel dimensions. Because these experimental parameters are closely related to Π_J, they allowed the identification of a meaningful range of variation for Π_J. For typical operating conditions of NF/RO single channels: $\mathrm{Re}_{p0} < 0.2$ and $\Delta_0 < 0.3$, thus $\Pi_{J,\max}$ was assigned to the maximum of $0.2/[\mathrm{Re}(1 - R\Pi_P]$ and $0.3/[2(L/h)(1 - R\Pi_P]$, as derived in Appendix C.

The CFD simulations run for a set of fixed parameters, that is, $h = 2$ mm, $\mu = 10^{-3}$ Pa·s, $\rho = 10^3$ kg/m^3, $\rho_{A0} = 1.0$ kg/m^3, $\Delta P = 10^6$ Pa, and $P_0 = 10^6$ Pa (relative pressure), whereas the remaining parameters—u_0, D_{AB}, L, R, b, and L_p—were varied to match the dimensionless numbers listed in Table 1.

Results

Figure 3 displays the CFD predictions (points) of Ξ vs. ϕ, for $R = 1.0$, $\Pi_P = 0.0$,** and the values of Re, Sc, L/h, and Π_J shown in Table 1. Sh^0 was calculated by the well-known Lévêque correlation: $\mathrm{Sh}^0 = 1.47(\mathrm{ReSc}\, h/L)^{1/3}$ (developed by Lévêque[18] and experimentally validated by Pickett and Stanmore[19]). The correction factor to obtain Sh at high mass-transfer rates, $\Xi \equiv \mathrm{Sh}/\mathrm{Sh}^0$, is clearly just a function of $\phi \equiv \mathrm{Pe}/\mathrm{Sh}^0$. Equation 13 was fitted to the CFD predictions by minimizing the maximum relative deviation of Ξ. The relationship determined, $\Xi = \phi + (1 + 0.58\phi^{1.6})^{-0.9}$, fits the CFD predictions very well with a maximum error of 5.9% and an average error of 1.8%.

The CFD predictions (points) of $\bar{\Gamma}$ vs. ϕ, for $R = 1.0$ and $\Pi_P = 0.0$, are shown in Figure 4. The average concentration polarization index $\bar{\Gamma}$ is solely correlated with ϕ, as well. The relationship $\Xi = \phi + (1 + 0.58\phi^{1.6})^{-0.9}$ (Figure 4, curve 1) adequately fits the CFD predictions of $\bar{\Gamma}$ with a maximum error lower than about 6% for $\phi < 4$; however, the error steeply increases for $\phi > 4$. At first sight, this relationship should fit well the CFD predictions of $\bar{\Gamma}$ for any ϕ because it fits the CFD predictions of Ξ very well. The reason for this unexpected discrepancy results from the fact that Eq. 14 for $R = 1$, that is, $\bar{\Gamma} = 1/(\Xi/\phi - 1)$, strongly magnifies the relative error of Ξ/ϕ as ϕ increases and $\Xi/\phi \to 1$. To overcome this problem, another relation $\Xi(\phi)$ was determined by minimizing the maximum relative deviation between $\bar{\Gamma}$ predicted by CFD and computed by Eq. 14, yielding a maximum error of 14% and an average error of 3.6% (Figure 4, curve 2):

$$\Xi = \phi + (1 + 0.26\phi^{1.4})^{-1.7} \tag{23}$$

This relationship was also plotted in Figure 3 and a perfect matching with CFD predictions (points) was observed, as well.

The mass-transfer correction factor Ξ, determined for $R = 1.0$ and $\Pi_P = 0.0$ (Eq. 23), is also adequate to predict $\bar{\Gamma}$ for the

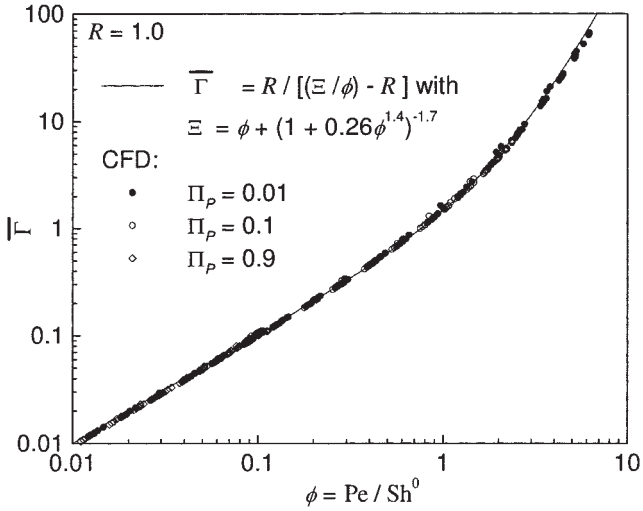

Figure 6. Comparison of $\bar{\Gamma}$ predicted by Eq. 23 with the CFD predictions (points) for $R = 1.0$; $\Pi_P = 0.01$, 0.1, and 0.9; and the dimensionless numbers (Re, Sc, L/h, Π_J) listed in Table 1.

** The condition $\Pi_P = 0$ corresponds to the permeation of an extremely dilute solution, the osmotic pressure of which is practically null, and thus the local permeation flux is nearly constant along the channel.

Table 2. Mass-Transfer Correlations for UF/RO Rectangular, Tubular, and Radial Crossflow Cells: (a) De and Bhattacharya[5] and (b) Minnikanti et al.[6]

Flow Regime and System Geometry	Theoretical Mass Transfer Correlation without Suction	Theoretical Mass-Transfer Correlation with Suction	Approximate Mass-Transfer Correlation with Suction
Laminar flow[(a)]			
Rectangular crossflow cell	$Sh^0_{de} = 1.85(Re_{de}Sc\ d_e/L)^{1/3}$	$Sh_{de} = 2.381\dfrac{(Re_{de}Sc\ d_e/L)^{1/3}}{I}$, where $I = \int_0^\infty \exp\left(-\dfrac{\eta^3}{3} - 0.42\lambda\eta\right)d\eta$ and $\lambda = \dfrac{Pe}{(Re_{de}Sc\ d_e/L)^{1/3}}$	$Sh_{de} = Sh^0_{de}(1.0 + 0.32\lambda + 0.02\lambda^2 - 8.05 \times 10^{-4}\lambda^3)$, for $\lambda < 10$
Tubular module	$Sh^0_d = 1.62(Re_dSc\ d/L)^{1/3}$	$Sh_d = 1.5\dfrac{(Re_dSc\ d/L)^{1/3}}{I}$, where $I = \int_0^\infty \exp\left(-\dfrac{8\eta^3}{9} - \dfrac{2}{3}\lambda\eta\right)d\eta$ and $\lambda = \dfrac{Pe}{(Re_dSc\ d/L)^{1/3}}$	$Sh_d = Sh^0_d(1.0 + 0.37\lambda + 0.03\lambda^2 - 1.05 \times 10^{-3}\lambda^3)$, for $\lambda < 10$
Radial cross-flow cell*	$Sh^0_h = 1.467(Re_hSc\ h/R)^{1/3}$	$Sh_h = 2.381\dfrac{(Re_hSc\ h/R)^{1/3}}{I}$, where $I = \int_0^\infty \exp\left(-\dfrac{\eta^3}{6} - 0.42\lambda\eta\right)d\eta$ and $\lambda = \dfrac{Pe}{(Re_hSc\ h/R)^{1/3}}$	$Sh_h = Sh^0_h(1.0 + 0.41\lambda + 0.03\lambda^2 - 1.25 \times 10^{-3}\lambda^3)$, for $\lambda < 10$
Turbulent flow[(b)]			
Tubular module or rectangular cell	$Sh^0_{de} = 0.275(Re^{1.75}_{de}Sc\ d_e/L)^{1/3}$	$Sh_{de} = 0.354\dfrac{(Re^{1.75}_{de}Sc\ d_e/L)^{1/3}}{I}$, where $I = \int_0^\infty \exp\left(-\dfrac{\eta^3}{3} - 2.82\lambda\eta\right)d\eta$ and $\lambda = \dfrac{Pe}{(Re^{1.75}_{de}Sc\ d_e/L)^{1/3}}$	$Sh_{de} = Sh^0_{de}(1.0 + 2.621\lambda + 0.443\lambda^2 - 8.73 \times 10^{-2}\lambda^3 + 8.833 \times 10^{-3}\lambda^4 - 4.417 \times 10^{-4}\lambda^5 + 8.676 \times 10^{-6}\lambda^6)$ for $\lambda < 15$
Radial crossflow cell**	$Sh^0_{de} = 0.22(Re^{1.75}_{de}Sc\ d_e/R)^{1/3}$	$Sh_{de} = 0.2832\dfrac{(Re^{1.75}_{de}Sc\ d_e/R)^{1/3}}{I}$, where $I = \int_0^\infty \exp\left(-\dfrac{\eta^3}{3} - 3.53\lambda\eta\right)d\eta$ and $\lambda = \dfrac{Pe}{(Re^{1.75}_{de}Sc\ d_e/R)^{1/3}}$	$Sh_{de} = Sh^0_{de}(1.0 + 3.415\lambda + 0.483\lambda^2 - 7.77 \times 10^{-2}\lambda^3 + 10.0 \times 10^{-3}\lambda^4 - 5.06 \times 10^{-4}\lambda^5 + 10.0 \times 10^{-6}\lambda^6)$ for $\lambda < 15$

Notes: L is the length of the slit or tube, R is the radius of the radial cell, d_e is the equivalent diameter (4 × ratio of the cell volume to the wetted surfaces area), h is half of the radial cell height. Sh and Re subscripts refer to their characteristic dimensions.
* The characteristic velocity in Re is the average velocity at the radial cell outlet.
**The characteristic velocity in Re is the radial average of the mean velocity along the radial cell.

remaining values of R and Π_P displayed in Table 1: $0.10 \le R \le 0.999$ and $0.01 \le \Pi_P \le 0.9$, with a maximum error of 18% and an average error of 3.2%. The data of $\bar{\Gamma}$ predicted by CFD and computed by Eqs. 14 and 23 are plotted in Figure 5, for $\Pi_P = 0.0$ and $0.10 \le R \le 0.99$, and in Figure 6 for $R = 1.0$ and $\Pi_P = 0.01$, 0.1, and 0.9. An excellent agreement is observed in both figures, suggesting that the mass-transfer correction factor, $\Xi(\phi)$, may be determined for other NF/RO systems solely based on CFD predictions or experimental data determined for $R = 1.0$ and $\Pi_P = 0.0$ (permeation of dilute solutions through ideal selective membranes).

Discussion

As mentioned earlier, the relationship $\Xi(\phi)$ that fitted the CFD predictions of $\bar{\Gamma}$ for $R = 1.0$ and $\Pi_P = 0.0$ is also suitable

Table 3. Mass-Transfer Correction Factors Derived from the Mass-Transfer Correlations in Table 2*

Flow Regime and System Geometry	Analytical Equation with Numerical Coefficients	Eq.	Approximate Mass-Transfer Correction Factor	Validity Range	Eq.
Laminar flow					
Rectangular cell	$\Xi = \dfrac{0.99983}{\int_0^\infty \exp(-0.71058\eta^3 - \phi\eta)d\eta}$	(24)	$\Xi = 1.0 + 0.592\phi + 0.06845\phi^2 - 5.097 \times 10^{-3}\phi^3$	$\phi < 5.4$	(29)
Tubular module	$\Xi = \dfrac{0.999546}{\int_0^\infty \exp(-0.70562\eta^3 - \phi\eta)d\eta}$	(25)	$\Xi = 1.0 + 0.5994\phi + 0.078732\phi^2 - 4.4641 \times 10^{-3}\phi^3$	$\phi < 6.2$	(30)
Radial cell	$\Xi = \dfrac{1.00002}{\int_0^\infty \exp(-0.71254\eta^3 - \phi\eta)d\eta}$	(26)	$\Xi = 1.0 + 0.60147\phi + 0.064563\phi^2 - 3.9464 \times 10^{-3}\phi^3$	$\phi < 6.8$	(31)
Turbulent flow					
Tubular module or rectangular cell	$\Xi = \dfrac{0.99829}{\int_0^\infty \exp(-0.71471\eta^3 - \phi\eta)d\eta}$	(27)	$\Xi = 1.0 + 0.72078\phi + 0.033502\phi^2 - 1.8156 \times 10^{-3}\phi^3 + 5.0517 \times 10^{-5}\phi^4 - 6.94690 \times 10^{-7}\phi^5 + 3.75246 \times 10^{-9}\phi^6$	$\phi < 54.5$	(32)
Radial cell	$\Xi = \dfrac{0.99969}{\int_0^\infty \exp(-0.71169\eta^3 - \phi\eta)d\eta}$	(28)	$\Xi = 1.0 + 0.7513\phi + 0.023377\phi^2 - 8.2735 \times 10^{-4}\phi^3 + 2.34256 \times 10^{-5}\phi^4 - 2.60774 \times 10^{-7}\phi^5 + 1.1338 \times 10^{-9}\phi^6$	$\phi < 68.2$	(33)

Note: The equations and validity ranges presented here were derived through the substitution of Sh and λ by Ξ and ϕ, respectively, in the corresponding equations and validity ranges shown in Table 2.
*From De and Bhattacharya[5] and Minnikanti et al.[6]

to predict $\bar{\Gamma}$ for $0.10 \le R \le 0.999$ and $0.01 \le \Pi_P \le 0.9$. This fact suggests that the average concentration polarization index for a given membrane module can be determined based on a mass-transfer correlation at low mass-transfer rates (Sh^0) and a correction factor Ξ, which is just a function of ϕ.

A mass-transfer correction factor was first derived by Ackermann[20] and Colburn and Drew,[21] by using the film theory: $\Xi = \phi + \phi/[\exp(\phi) - 1]$, as quoted by Krishna.[22] The film theory matches the CFD predictions of Ξ very well indeed (Figure 3).† However, it matches the CFD predictions of $\bar{\Gamma}$ only for $\phi < 1$ (Figure 4, curve 3), the error increasing to roughly 15% at $\phi = 1$, that is, the film theory is definitely inadequate to predict $\bar{\Gamma}$ for $\phi > 1$. In any case, claiming that the film theory cannot predict the concentration polarization index in NF/RO systems[5,6,23] is not entirely correct. Despite its simplicity, the film theory is suitable for design purposes as long as $\phi < 1$ (low suction).

To validate the hypothesis that $\Xi(\phi)$ is independent of the membrane module geometry and flow regime, the mass-transfer correlations of Sh at low and high mass-transfer rates developed by De and Bhattacharya[5] and Minnikanti et al.[6] for several module geometries and flow regimes (Table 2) were analyzed. The Sh theoretical mass-transfer correlations with suction were derived for pressure-driven membrane processes and binary solutions by solving analytically the solute transport equation, and assuming steady state, fully developed flow, constant physical properties and ideal membranes ($R = 1$). Because these theoretical correlations require the numerical calculation of an integral expression, those authors[5,6] opted for Sh polynomial approximations instead.

Based on the Sh theoretical mass-transfer correlations with suction,[5,6] we derived the corresponding Ξ expressions (Table 3). Surprisingly, the analytical equations of Ξ (Eqs. 24–28) are very similar. As a matter of fact, these equations are distinct approximations of Eq. 34, the latter of which was also derived in this work right from the beginning for the five systems by a strict mathematical handling (with the help of the software Maple V Release 5.1), without making numerical approximations of the coefficients as did De and Bhattacharya[5] and Minnikanti et al.[6]:

$$\Xi = \frac{1}{\int_0^\infty \exp\left[-\dfrac{8\sqrt{3}\pi^3}{243\Gamma^3(2/3)}\eta^3 - \eta\phi\right]d\eta} = \frac{1}{\int_0^\infty \exp(-0.71207\eta^3 - \eta\phi)d\eta} \quad (34)$$

where Γ is the gamma function. Equation 34 confirms that the mass-transfer correction factor Ξ depends only on ϕ, and it is independent of the membrane module geometry and flow regime.

Figure 7 compares $\bar{\Gamma}$ data predicted by Eqs. 23 (semiempirical correction factor determined in this work, curve 1), 34 (theoretical correction factor, curve 2), and 29–33 (approximate correction factors, curves 3–7). Equations 23 and 34

† Bird et al.[13] considered "high mass-transfer rates" whenever the magnitude of Ξ is >1 and reported studies for $1 < \Xi < 10$. The present study focused on a broader range: $1 < \Xi < 21$ (Figure 3).

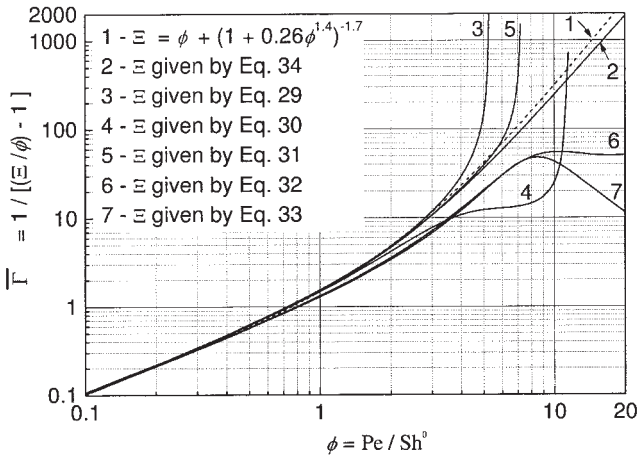

Figure 7. Comparison of $\bar{\Gamma}$ predicted by Eq. 23 (semiempirical correction factor determined in this work), Eq. 34 (theoretical correction factor), and Eqs. 29–33 (approximate correction factors), for $R = 1.0$.

predict similar $\bar{\Gamma}$ data for $\phi < 20$; however, the deviation between them increases to roughly 30% for $\phi = 20$. Equation 34 underestimates $\bar{\Gamma}$ because the underlying model takes a few assumptions not mandatory for the CFD model, such as linear velocity distribution $u(y)$ and negligible longitudinal variation of the diffusive flux, for example. The mass-transfer correction factor determined in this work (Eq. 23) should be used for membrane module design because it results from a more accurate model than those developed by De and Bhattacharya[5] and Minnikanti et al.[6] (Eqs. 24–28, Table 3). On the other hand, not one of the polynomial approximations of Ξ (Eqs. 29–33, Table 3) is valid for predicting $\bar{\Gamma}$ for the whole range of ϕ shown in Figure 7 ($\phi < 20$) and their validity ranges should be revised.

Conclusions

In the present work, a generalized mass-transfer correction factor Ξ was obtained to correct mass-transfer coefficients at impermeable walls and low mass-transfer rates, found to be independent of the membrane module geometry and the flow regime: $\Xi = \phi + (1 + 0.26\phi^{1.4})^{-1.7}$ with $\phi = \mathrm{Pe}/\mathrm{Sh}^0$. Unlike the correction factors available in the literature, it accurately predicts the average concentration polarization index for $\phi < 20$.

Because Ξ appears to be independent of the module geometry and the flow regime, to predict the average concentration polarization index for the design and optimization of new membrane modules with complex geometries, only a suitable correlation of $\mathrm{Sh}^0 = f(\mathrm{Re}, \mathrm{Sc}, \text{dimensions ratio})$ must be found and corrected by the mass-transfer correction factor developed in the present work.

Notation

b = parameter: $\pi = b\rho_A$, Pa m^3 kg^{-1}
c_1, c_2, c_3 = positive fitting parameters
D_{AB} = mass diffusivity, m^2/s
h = channel height, m
j_{Am} = local back-diffusion flux of solute A normal to the membrane surface, kg m^{-2} s^{-1}
$\bar{j}_{Am}$ = average back-diffusion flux of solute A normal to the membrane surface between $x = 0$ and $x = L$, kg m^{-2} s^{-1}
J_v = local permeate volumetric flux (or local permeate velocity), m/s
$\bar{J}_v$ = average permeate volumetric flux (or average permeate velocity), m/s
J_{v0} = permeate volumetric flux at the channel inlet, m/s
k_p = average mass-transfer coefficient, m/s
L = channel length, m
L_p = pure water hydraulic permeability, m s^{-1} Pa^{-1}
n_{Am} = local mass flux of solute A at the membrane surface with respect to stationary axes, kg·m^{-2} s^{-1}
n_{Ap} = local mass flux of solute A in the permeate stream with respect to stationary axes, kg·m^{-2} s^{-1}
P = hydraulic pressure, Pa
P^* = dimensionless hydraulic pressure
P_0 = hydraulic pressure at the channel inlet, Pa
Pe = average permeation Peclet number, $\mathrm{Pe} = \bar{J}_v h/D_{AB}$
R = intrinsic rejection, $R = (\rho_{Am} - \rho_{Ap})/\rho_{Am}$
R_{obs} = average observed rejection, $R_{obs} = (\rho_{A0} - \bar{\rho}_{Ap})/\rho_{A0}$
Re = Reynolds number at the channel inlet, $\mathrm{Re} = \rho u_0 h/\mu$
Re_{p0} = permeation Reynolds number at the channel inlet, $\mathrm{Re}_{p0} = \rho h J_{v0}/\mu$
Sc = Schmidt number, $\mathrm{Sc} = \mu/(\rho D_{AB})$
Sh = average Sherwood number, $\mathrm{Sh} = k_p h/D_{AB}$
Sh^0 = Sherwood number for vanishing mass-transfer rates at impermeable walls
u = crossflow velocity, m/s
u^* = dimensionless crossflow velocity, $u^* = u/u_0$
u_0 = average crossflow velocity at the channel inlet, m/s
v = velocity normal to the membrane surface, m/s
v^* = dimensionless velocity normal to the membrane surface, $v^* = v/u_0$
W = channel width, m
x = distance to the channel inlet, m
x^* = dimensionless distance to the channel inlet, $x^* = x/h$
y = distance to the channel axis, m
y^* = dimensionless distance to the channel axis, $y^* = y/h$

Greek letters

Δ_0 = water recovery rate at the channel inlet, $\Delta_0 = 2J_{v0}L/(u_0 h)$
ΔP = transmembrane pressure, Pa
ϕ = ratio of the permeation Peclet number to the Sherwood number for vanishing mass-transfer rates at impermeable walls, $\phi = \mathrm{Pe}/\mathrm{Sh}^0$
Γ = gamma function
$\bar{\Gamma}$ = average concentration polarization index, $\bar{\Gamma} = (\bar{\rho}_{Am} - \rho_{A0})/\rho_{A0}$
η = integration variable in Eq. 34
μ = dynamic viscosity, Pa·s
π = osmotic pressure, Pa
π_0 = osmotic pressure at the channel inlet, Pa
Π_P = dimensionless osmotic pressure, $\Pi_P = \pi_0/\Delta P$
Π_J = dimensionless pure water flux, $\Pi_J = L_p \Delta P/u_0$
Ξ = correction factor by which Sh^0 must be multiplied to obtain Sh at high mass-transfer rates, $\Xi = \mathrm{Sh}/\mathrm{Sh}^0$
ρ = density, kg/m^3
ρ_A = mass concentration of solute A, kg/m^3
ρ_A^* = dimensionless mass concentration of solute A, $\rho_A^* = \rho_A/\rho_{A0}$
ρ_{A0} = mass concentration of solute A in the feed stream, kg/m^3
ρ_{Am} = mass concentration of solute A at the membrane surface, kg/m^3
$\bar{\rho}_{Am}$ = permeate flux-average mass concentration of A at the membrane surface, kg/m^3
ρ_{Ap} = mass concentration of solute A in the permeate stream, kg/m^3
$\bar{\rho}_{Ap}$ = permeate flux-average mass concentration of A in the permeate stream, kg/m^3
ξ = function in Eqs. 12 and 13, $\Xi = \phi + \{1/[1 + \xi(\phi)]^{c1}\}$, with $\xi(\phi) = c_2 \phi^{c3}$

Literature Cited

1. Sherwood TK, Brian PLT, Fisher RE, Dresner L. Salt concentration at phase boundaries in desalination by reverse osmosis. *Ind Eng Chem Fundam.*1965;4:113-8.
2. Rautenbach R, Albrecht R. *Membrane Processes*. New York: Wiley; 1989.
3. Bhattacharyya D, Williams ME. Part VI—Reverse osmosis, Chapter 22: Theory. In Ho WSW, Sirkar KK, eds. *Membrane Handbook*. New York: Van Nostrand Reinhold; 1992:269-280.
4. Gekas V, Ölund K. Mass transfer in the membrane concentration polarization layer under turbulent cross flow. II. Application to the characterization of ultrafiltration membranes. *J Membr Sci.* 1988;37: 145-163.
5. De S, Bhattacharya PK. Prediction of mass-transfer coefficient with suction in the applications of reverse osmosis and ultrafiltration. *J Membr Sci.* 1997;128:119-131.
6. Minnikanti VS, DasGupta S, De S. Prediction of mass-transfer coefficient with suction for turbulent flow in cross flow ultrafiltration. *J Membr Sci.*1999;157:227-239.
7. van den Berg GB, Rácz IG, Smolders CA. Mass transfer coefficients in cross-flow ultrafiltration. *J Membr Sci.* 1989;47:25-51.
8. Zydney AL. Stagnant film model for concentration polarization in membrane systems. *J Membr Sci.*1997;130:275-281.
9. Miranda JM, Campos JBLM. Mass transfer in the vicinity of a separation membrane—The applicability of the stagnant film theory. *J Membr Sci.* 2002;202:137-150.
10. Wiley DE, Fletcher DF. Computational fluid dynamics modelling of flow and permeation for pressure-driven membrane processes. *Desalination.* 2002;145:183-186.
11. Geraldes V, Semião V, de Pinho MN. Concentration polarisation and flow structure within nanofiltration spiral-wound modules with ladder-type spacers. *Comput Struct.* 2004;82:1561-1568.
12. Ghidossi R, Veyret D, Moulin P. Computational fluid dynamics applied to membranes: State of the art and opportunities. *Chem Eng Process.* 2006;45:437-454.
13. Bird RB, Stewart WE, Lightfoot EN. *Transport Phenomena*. 2nd Edition. New York: Wiley; 2002.
14. Patankar SV. *Numerical Heat Transfer and Fluid Flow*. New York: Hemisphere Publishing/McGraw-Hill; 1980.
15. Geraldes V, Semião V, de Pinho MN. Numerical modelling of mass transfer in slits with semi-permeable membrane walls. Engineering computations. *Int J Comput-Aided Eng Software.* 2000;17:192-217.
16. Berman AS. Laminar flow in channels with porous walls. *J Appl Phys.* 1953;24:1232-1235.
17. Davies SJ, White CM. An experimental study of the flow of water in pipes of rectangular section. *Proc R Soc Lond A Phys Sci.*1928;119: 92-107.
18. Lévêque MA. Les lois de la transmission de chaleur par convection. *Ann Mines.* 1928;13:201-415.
19. Pickett DJ, Stanmore BR. Ionic mass transfer in parallel plate electrochemical cells. *J Appl Electrochem.*1972;2:151-6.
20. Ackermann G. Wärmeübergang und molekulare Stoffübertragung im gleichen Feld bei großen Temperatur- und Partialdruckdifferenzen. *Ver Dtsch Ingen Forsch.*1937;382:1.
21. Colburn AP, Drew TB. The condensation of mixed vapors. *Trans AIChE.* 1937;33:197.
22. Krishna R. Mass and heat transfer to spheres, cylinders and planar surfaces: A unified "film" model description. *Int Commun Heat Mass Transfer.* 2001;28:39-48.
23. Gekas V, Hallström B. Mass transfer in the membrane concentration polarization layer under turbulent cross flow. I. Critical literature review and adaptation of existing Sherwood correlations to membrane operations. *J Membr Sci.* 1987;30:153-170.

Appendix A: Permeate Flux-Averages

The local mass flux of solute A at the membrane surface n_{Am} is related to j_{Am} as[13]

$$n_{Am} = J_v \rho_{Am} + j_{Am} \tag{A1}$$

where J_v is the local permeate flux and j_{Am} is the local back-diffusion flux of solute A. Assuming unhindered transport of the solute in the permeate side, at steady state, n_{Am} equals the local mass flux of solute A in the permeate, n_{Ap}, given by

$$n_{Ap} = J_v \rho_{Ap} \tag{A2}$$

The permeate flux-average mass concentration of A at the membrane surface, $\bar{\rho}_{Am}$, is defined as

$$\bar{\rho}_{Am} = \frac{\int_0^L J_v \rho_{Am} dx}{\int_0^L J_v dx} \tag{A3}$$

Assuming that the intrinsic rejection R is independent of x, the permeate flux-average mass concentration of A in the permeate stream, $\bar{\rho}_{Ap}$, is given by

$$\bar{\rho}_{Ap} = \frac{\int_0^L J_v \rho_{Ap} dx}{\int_0^L J_v dx} = \frac{\int_0^L J_v (1-R) \rho_{Am} dx}{\int_0^L J_v dx} = (1-R)\bar{\rho}_{Am} \tag{A4}$$

On the other hand, the permeate flux-average back-diffusion flux of A, $\bar{j}_{Am}$, is

$$\begin{aligned} \bar{j}_{Am} &= \frac{1}{L}\int_0^L j_{Am} dx = -\frac{1}{L}\int_0^L J_v(\rho_{Am} - \rho_{Ap}) dx \\ &= -\frac{\int_0^L J_v dx}{L} \frac{\int_0^L J_v(\rho_{Am} - \rho_{Ap}) dx}{\int_0^L J_v dx} \\ &= -\bar{J}_v \left(\frac{\int_0^L J_v \rho_{Am} dx}{\int_0^L J_v dx} - \frac{\int_0^L J_v \rho_{Ap} dx}{\int_0^L J_v dx} \right) = -\bar{J}_v(\bar{\rho}_{Am} - \bar{\rho}_{Ap}) \end{aligned} \tag{A5}$$

Appendix B: Dimensionless Analysis

By inserting the dimensionless variables $x^* = x/h$, $y^* = y/h$, $u^* = u/u_0$, $v^* = v/u_0$, $\rho_A^* = \rho_A/\rho_{A0}$, and $P^* = (P - P_0)/(\rho u_0^2)$, the differential Eqs. 15–18 become

$$\frac{\partial u^*}{\partial x^*} + \frac{\partial v^*}{\partial y^*} = 0 \tag{B1}$$

$$u^* \frac{\partial u^*}{\partial x^*} + v^* \frac{\partial u^*}{\partial y^*} = -\frac{\partial P^*}{\partial x^*} + \frac{1}{\mathrm{Re}}\left[\frac{\partial^2 u^*}{\partial x^{*2}} + \frac{\partial^2 u^*}{\partial y^{*2}}\right] \tag{B2}$$

$$u^* \frac{\partial v^*}{\partial x^*} + v^* \frac{\partial v^*}{\partial y^*} = -\frac{\partial P^*}{\partial y^*} + \frac{1}{\mathrm{Re}}\left[\frac{\partial^2 v^*}{\partial x^{*2}} + \frac{\partial^2 v^*}{\partial y^{*2}}\right] \tag{B3}$$

$$u^* \frac{\partial \rho_A^*}{\partial x^*} + v^* \frac{\partial \rho_A^*}{\partial y^*} = \frac{1}{\mathrm{Re\ Sc}}\left[\frac{\partial^2 \rho_A^*}{\partial x^{*2}} + \frac{\partial^2 \rho_A^*}{\partial y^{*2}}\right] \tag{B4}$$

and the boundary conditions (Eqs. 19–22) become

- at $y^* = 1/2$ and $x^* > 0$

$$u^* = 0 \qquad v^* = \Pi_J(1 - R\Pi_P \rho_{Am}^*)$$
$$\partial \rho_A^*/\partial y^* = \mathrm{Re\ Sc} R v^* \rho_{Am}^* \tag{B5a,b,c}$$

- at $y^* = 0$ and $x^* > 0$

$$\partial u^*/\partial y^* = 0 \qquad v^* = 0 \qquad \partial \rho_A^*/\partial y^* = 0 \tag{B6a,b,c}$$

- at $x^* = 0$ and $0 < y^* < 1/2$

$$u^* = \frac{3}{2}[1 - (2y^*)^2] \qquad v^* = 0 \qquad \rho_A^* = 1 \qquad P^* = 0 \tag{B7a,b,c,d}$$

- at $x^* = L/h$ and $0 < y^* < 1/2$

$$\partial u^*/\partial x^* \approx 0 \qquad \partial v^*/\partial x^* = 0 \qquad \partial \rho_A^*/\partial x^* \approx 0 \tag{B8a,b,c}$$

where $\mathrm{Re} = \rho u_0 h/\mu$ is the Reynolds number, $\mathrm{Sc} = \mu/(\rho D_{AB})$ is the Schmidt number, $\Pi_J = L_p \Delta P/u_0$ (dimensionless pure water flux), and $\Pi_P = \pi_0/\Delta P$ (dimensionless osmotic pressure).

Appendix C: Maximum Limits of Π_J

For typical operating conditions of NF/RO single channels:

$$\mathrm{Re}_{p0} = \frac{\rho h J_{v0}}{\mu} < 0.2 \Leftrightarrow J_{v0} < \frac{0.2\mu}{\rho h} \tag{C1}$$

$$\Delta_0 = \frac{(\text{flow rate})_{\text{permeate}}}{(\text{flow rate})_{\text{feed}}} = \frac{2LWJ_{v0}}{hWu_0} = \frac{2J_{v0}L}{u_0 h} < 0.3 \Leftrightarrow \frac{J_{v0}}{u_0} < \frac{0.3h}{2L} \tag{C2}$$

On the other hand, according to Eq. B5b and bearing in mind that $\rho_{Am}^* = 1$ at the membrane inlet edge ($y^* = 1/2$, $x^* = 0$):

$$v^* = \frac{J_{v0}}{u_0} = \Pi_J(1 - R\Pi_P) \Leftrightarrow \Pi_J = \frac{J_{v0}/u_0}{1 - R\Pi_P} \tag{C3}$$

Substituting Eqs. C1 and C2 into Eq. C3 yields the maximum limits of Π_J:

$$\Pi_J < \frac{\dfrac{0.2\mu}{\rho h u_0}}{1 - R\Pi_P} = \frac{0.2}{\mathrm{Re}(1 - R\Pi_P)} \tag{C4}$$

$$\Pi_J < \frac{\dfrac{0.3h}{2L}}{1 - R\Pi_P} = \frac{0.3}{2L/h(1 - R\Pi_P)} \tag{C5}$$

Manuscript received Jun. 2, 2005, and revision received Jun. 24, 2006.